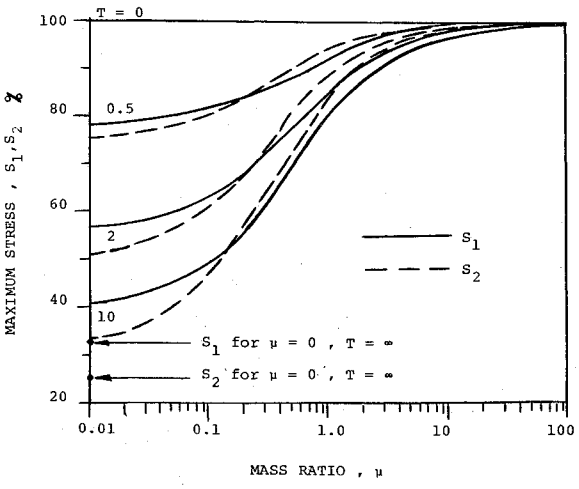

Fig. 2 Maximum bending stress due to inertial loads.

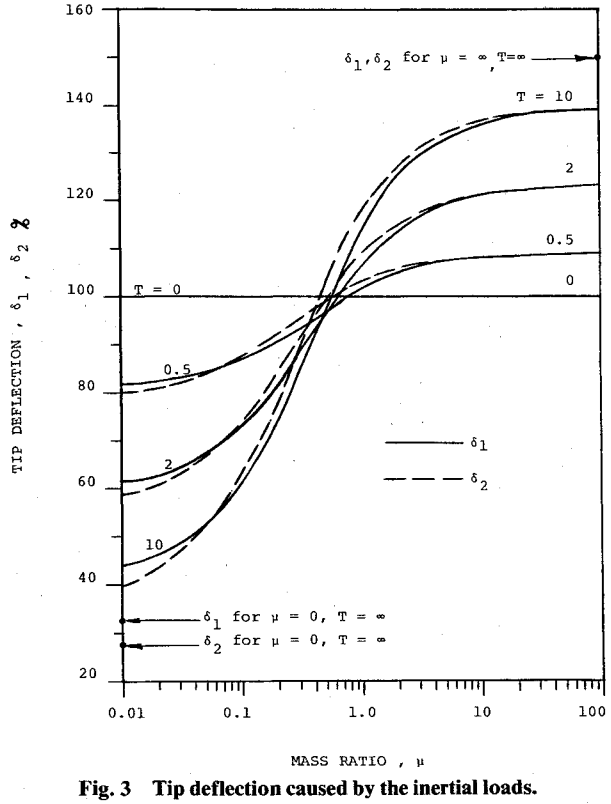

Fig. 3 Tip deflection caused by the inertial loads.

is complicated. However, based on physical considerations[5], the following expression for apparent thermal bending moment was established

$$M=\beta Eed^4J\alpha/k \qquad (5)$$

Where β is a constant depending upon the boom section geometry and its oreitnation with respect to the sun.

If the boom is free to expand and contract, the moment M results in thermal bending and no stresses develop. A restrained thermal expansion of the boom results in stresses but the amount of thermal bending is reduced depending upon the amount of restraint. Considering no restraints, the maximum tip deflection has been obtained by using Eq. (5) and beam bending theory

$$\delta_t=200(1+T)\,[T-\log_e(1+T)\,]/T^2 \qquad (6)$$

As $T\to\infty$, $\delta_t\to 200\%$. It should be noticed that this deflection does not depend upon the tip mass.

d) Weight of the boom: The weight of a linearly thickness-tapered boom as a percentage weight of a uniform boom of thickness t_1 can be expressed as

$$W=50(2+T)/(1+T) \qquad (7)$$

As $T\to\infty$, $W\to 50\%$.

Results and Discussion

Equations (1-6) can be utilized to compare the mechanical performance of a linearly thickness-tapered boom with a uniformly thick boom when the application involves supporting a mass at the tip. Figure 2 gives the maximum bending stress experienced by the tapered boom as a percentage of the corresponding stress of a uniformly thick boom under constant and linearly varying acceleration loads. It can be seen that for low-mass ratios these stresses are significantly lower than the values for a uniform boom. Even for high-mass ratios, the stress values never exceed the values for uniform boom for any thickness parameter T. The maximum deflection caused by the inertial loads has been plotted as a function of mass ratio in Fig. 3 for different values of the thickness parameter. The advantage of the thickness-tapered boom in terms of tip deflection can be seen only for mass ratio of less than 0.5. However, even for high-mass ratio and high-thickness parameter ($\mu\to\infty$ and $T\to\infty$), the deflection value is not more than 50% higher than that of a uniform boom. The variation in the maximum thermal deflection as a function of the thickness parameter is given by Eq. (6). The deflection increases as the taperness of the boom is increased. As $T\to\infty$, the predicted value of thermal deflection approaches twice that of uniform boom. The advantage of the thickness-tapered boom in terms of weight reduction is evident from Eq. (7). It can be seen that maximum possible weight saving by using a linearly thickness-tapered boom is 50%.

The previous results indicate that a thickness-tapered boom can be used for supporting tip mass with the advantages of reduced bending stresses and saving in weight if the values of tip deflection are found to be within an allowable limit.

References

[1]Rimrott, F.P.J., "Storable Tubular Extendible Member-A Unique Machine Element," *Machine Design,* Vol. 37, Dec. 1965, pp. 156-168.

[2]Herzl, G.G., "Tubular Spacecraft Booms (Extendible, Reel Stored)," *Aerospace Mechanism Series,* Vol. 2, 1970.

[3]Kumar, R. and Ahmed, S., "Bending and Flexing of the Apollo 15 Mass Spectrometer Boom," *Journal of Spacecraft and Rockets,* Vol. 9, Dec. 1972, pp. 940-942.

[4]Kumar, R. and Ahmed, S., "Analysis of Thickness Tapered Booms for Space Applications," *Journal of Spacecraft and Rockets,* Vol. 11, Feb. 1974, pp. 125-127.

[5]Ahmed, S., Kumar, R., and Predmore, R.E., "Prediction of Solar Induced Response of Thin Walled Open Section Booms for Design," *Proceedings of the International Symposium on Experimental Mechanics,* Vol. I (Advance Copy), University of Waterloo, Waterloo, Ontario, Canada, 1972, pp. 22-1-22-14.

Graphic Representation of Superorbital Rocket Performance

Robert Sandri*
National Research Council of Canada

THIS note deals with the usefulness of the nuclear-thermal and high-energy chemical rocket drives in the last stage of multistage vehicles. Its purpose is to supplement and

Received November 5, 1975; revision received December 19, 1975.
Index categories: LV/M Mission Studies and Economics, Nuclear Propulsion.

*Consultant to the Mechanical Engineering Division of the National Research Council.

bring up to date an earlier note of the author dealing with the same topic (Ref. 1).

A specific impulse of 800 sec is assumed for the nuclear drive and 400 sec for the chemical drive (hydrogen-oxygen). The last stage will operate at superorbital velocity and gravity losses will not appreciably impair payload efficiency.

The performance of any rocket vehicle is characterized by three "mission parameters," namely velocity increase ΔV, initial weight W, and payload L. If any two of these parameters are given, the third can be found from a simple graph (Fig. 1).

To construct the graph, a suitable assumption concerning the weight of the rockets has to be made. The dry weight (excluding payload) of any vehicle using liquid propellants comprises one part A which, within wide limits, is independent of the propellant weight and another part which is proportional (by a constant B) to the propellant weight P. The constant weight component comprises engine, guidance and control system and part of the structure; the variable component comprises propellant tanks, tank pressurization system and part of the structure. The factor B can be calculated by methods described in Ref. 2.

In the following, the subscript "n" refers to the nuclear rocket and the subscript "c" to the chemical rocket. So the total initial weight of the nuclear rocket will be

$$W_n = A_n + B_n P_n + P_n + L \tag{1}$$

and that of the chemical rocket

$$W_c = A_c + B_c P_c + P_c + L \tag{2}$$

The nuclear propellant weight is related to the velocity increase by the equation

$$P_n = W_n[1 - \exp(-\Delta V/gI_n)] = W_n z \tag{3}$$

where I is the specific impulse. Substituting in Eq. (1) one finds

$$W_n = (A_n + L)/[1 - (1 + B_n)z] \tag{4}$$

where z is a function of velocity defined by Eq. (3). For the chemical rocket one has $I_c = \frac{1}{2} I_n$ and hence

$$P_c = W_c[1 - \exp(-\Delta V/gI_c)] = W_c z(2 - z) \tag{5}$$

and from Eq. (2)

$$W_c = (A_c + L)/[1 - (1 + B_c)z(2 - z)] \tag{6}$$

Equations (4) or (6) can be used to construct graphs of the family of curves $L = \text{const}$ by plotting W_n or W_c against z or against ΔV. Such graphs immediately give complete information on the performance of the nuclear or chemical rocket.

By comparing the two graphs one can also establish which drive is better for a given mission, e.g., which rocket can carry more payload for a given initial weight and velocity increase. However, for this purpose it is better to consolidate the graphs for the two drives into a single graph, as shown in Fig. 1.

The two rockets are equivalent if they have equal initial weights, carry equal payloads, and are accelerated by the same velocity increase.

Letting $W_c = W_n = W_e$ we find from Eqs. (4) and (6)

$$W_e = \alpha/z(\beta - z) \tag{7}$$

where

$$\alpha = (A_n - A_c)/(1 + B_c)$$

$$\beta = 1 - (B_n - B_c)/(1 + B_c)$$

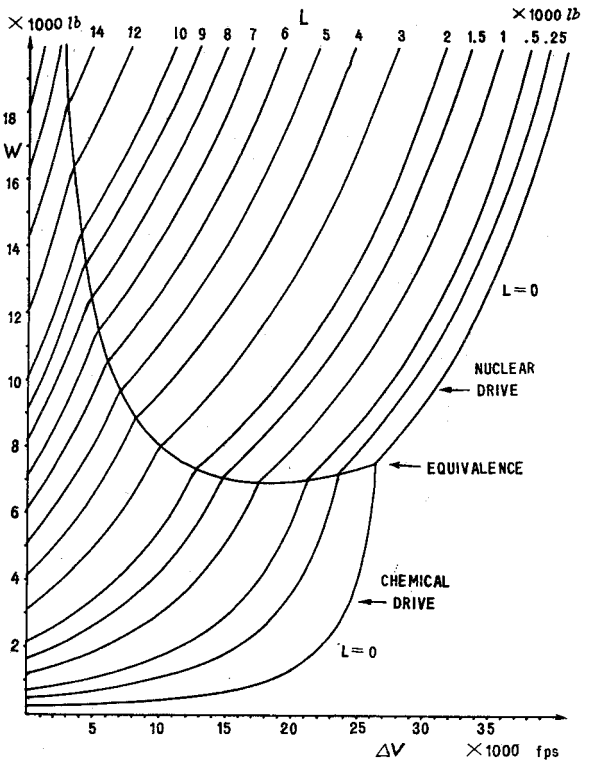

Fig. 1 Superorbital rocket performance.

The curve for "equivalence initial weight" W_e is plotted in Fig. 1. For rockets having an initial weight less than W_e, the chemical drive—owing to its lower engine weight— is better, otherwise the nuclear drive is better. So the equivalence curve separates areas of superiority of either drive.

Below the equivalence curve Eq. (6) is used for plotting the curves $L = \text{const}$, and above the equivalence curve Eq. (4) is used instead. The curve for $L = 0$ is of particular interest. Below it, the mission is impossible, i.e., neither of the two rockets under consideration can attain a given velocity increase ΔV if its initial weight is less than that corresponding to $L = 0$.

The graph shows immediately which drive is better and what it can achieve. For instance, let us assume that the initial weight is specified by the load capacity of the suborbital rocket stages and that the payload is also specified. Then the graph shows what velocity increase can be attained. If the payload is specified together with the velocity increase, the initial weight, of the rocket can be found from the graph. If the velocity increase is specified together with the initial weight, the payload can be found.

In constructing the graph it has been assumed that the propellant tanks are always filled to capacity. Therefore, the initial weight excluding payload of any given rocket vehicle is exactly known and from the graph it can easily be determined what the velocity increase will be for any payload added. (The altitude of the orbit from which the last stage starts will, of course, decrease somewhat with increasing payload but this is not significant.)

Figure 1 was drawn assuming the following numerical values: $A_n = 2100$ lb, $B_n = B_c = 0.125$, $A_c = 150$ lb, and $I_n = 2I_c = 800$ sec. In the calculation of B_c and B_n, a tank pressure of 100 psi was assumed for the chemical rocket (pressure-fed) and 30 psi for the nuclear rocket (pump-fed). The nuclear rocket has bulkier tanks than the chemical rocket but this is compensated by the lower tank pressure and reduced wall thickness. So one finds $B_n = B_c$. The weight A_n of the smallest practical nuclear rocket engine and likewise the weight A_c are, of course, somewhat arbitrary estimates. Figure 1 should therefore be regarded as an example rather than as a technical assessment.

The nuclear engine was assumed to give a thrust of 10,000 lb. The graph is broken off at an initial weight of 20,000 lb because beyond that limit, gravity losses are no longer negligible in the determination of payload efficiency. For practical application, the graph should be redrawn, to a larger scale, on graph paper.

The equivalence condition has been discussed more elaborately in Refs. 1 and 3. Graphs similar to Fig. 1 can also be constructed for the comparison of more than two rocket drives as was dealt with in Ref. 3.

References

[1]Sandri, R., "Nuclear-Thermal vs Chemical Drives for Super-Orbital Velocities," *Journal of Spacecraft and Rockets*, Vol. 1, Sept.-Oct. 1964, pp. 568-569.

[2]Sandri, R., "Some Considerations on the Use of a Pressurized Tank System for a Rocket Engine," *Canadian Aeronautics and Space Journal*, Vol. 13, Oct. 1967, pp. 369-372.

[3]Sandri, R., "An Efficiency Criterion for Super-Orbital Rocket Propulsion Systems," *Journal of Spacecraft and Rockets*, Vol. 5, Feb. 1968, pp. 217-218.

Cylindrical Diffuser Performance using a Truncated Plug Nozzle

Fred L. Galanga* and Thomas J. Mueller†
University of Notre Dame, Notre Dame, Ind.

Nomenclature

A = area
D = diameter
L = length
P = pressure
r = radius
x = axial distance from T-P nozzle exit

Subscripts

at = atmospheric conditions
b = plug base
cell = cell region
d = diffuser duct
ne = nozzle exit
nt = nozzle throat
p = plug
sh = nozzle shroud
01 = stagnation conditions

Introduction

CONVENTIONAL altitude facilities used to evaluate nozzle performance are generally equipped with simple exhaust diffusers that supplement facility exhausters.[1] Although flow models have been developed which are able to accurately predict diffuser performance characteristics using conventional bell nozzles, the performance of such systems using the altitude compensating truncated plug (T-P) nozzles has not been fully developed at present due to its complicated flowfield. This Note reviews some aspects of diffuser performance for a T-P nozzle without external flow.

Received August 29, 1975; revision received December 1, 1975. This research was jointly supported by NASA under contract NAS8-25601 and the Department of Aerospace and Mechanical Engineering, and was part of the M.S. thesis of the first author. The authors would like to thank R.J. Matz and R.C. Bauer of ARO, Inc., Tullahoma, Tennessee for their helpful comments throughout this investigation.

Index categories: Rocket Engine Testing; Airbreathing Engine Testing; Nozzle and Channel Flow.

*Research Assistant. Member AIAA.

†Professor. Associate Fellow AIAA.

General Features of Diffuser Operation

The process of achieving a reduced nozzle ambient or cell pressure with a supersonic nozzle and a cylindrical diffuser is relatively simple. The free-jet boundary emanating from the exit of a bell nozzle or the T-P nozzle, acts as a pump. Viscous shear along the jet boundary tends to pull the dead air from the cell region (Fig. 1) causing the plume to expand farther until it impinges on the diffuser wall. Here a quasi-steady-state condition is achieved; the cell pressure remains relatively constant while the impingement shock forms a complex shock system downstream, along with a static pressure rise in the diffuser. The condition of a very nearly constant cell pressure to upstream stagnation pressure ratio (P_{cell}/P_{01}) with changing overall (i.e., atmospheric to stagnation) pressure ratio (P_{at}/P_{01}) constitutes the "started" condition of the nozzle-diffuser system,[1] as opposed to the "unstarted" condition where cell pressure ratio varies with overall pressure ratio.

Equipment and Procedure

Tests were conducted using the Notre Dame blowdown Nozzle Thrust Facility (NTF). The T-P nozzle used (Fig. 1) was designed for an exit Mach number of 1.9 based on the overall nozzle exit to the throat area ratio. The nozzle shroud contour from the throat to the exit was cylindrical which fixed the nozzle exit angle at zero degrees. The plug was conical in shape from the throat and converged to the axis of symmetry at an angle of 10°. The base of the plug contained a central pressure tap to monitor the base pressure during all tests. A mating section was constructed to allow the diffuser to be bolted directly to the nozzle. The actual diffuser section was fashioned into two 13.97 cm lengths to facilitate boring of the duct diameter and to allow for testing of two different duct lengths. Six different duct diameters were evaluated during the tests. The diffuser was fitted with 39 sidewall taps to record pressure conditions from the cell region to the exit. A slotted hypotube was installed in its base to measure pressure distribution down the centerline of the diffuser. Twenty 150 cm mercury-filled manometers were used to record pressures.

Standard operating procedure for the NTF consisted of presetting the desired nozzle total pressure and then starting the flow. After allowing oscillations to damp, pressure conditions indicated by the manometers were photographically recorded. Shadowgraphs and total pressure measurements of the diffuser exit flow were also taken at this time.

Results

Figure 2 shows a typical centerline and sidewall pressure variation along the length of the duct. For this case the duct area to nozzle exit area ratio is 1.384. The approximate jet impingement point corresponding to the highest recorded wall pressure is 0.34 nozzle diam downstream of the nozzle exit. The pressure distribution down the duct indicates a shock wave system of diminishing strength occurring for about 5-6 nozzle exit diam downstream of the nozzle exit. This is borne out by the fact that where the centerline pressure ratio is a maximum, the sidewall pressure ratio corresponds to a minimum and vice versa. Beyond 6 nozzle exit diam, both the sidewall and the centerline static pressures show a gradual rise. Here the flow is still supersonic but decelerating. At the duct exit the sidewall pressure suddenly jumps indicating a shock wave (verified by shadowgraph pictures). Plug base pressures obtained with the hypotube installed were within 2% of the base pressures obtained[2] without the tube which suggests that tube interference effects were small.

Figures 3 and 4 show the variation of cell pressure ratio with overall pressure ratio for the long and short diffusers, respectively. With the longer diffuser (Fig. 3) it is evident that as the duct area ratio increases the cell pressure ratio decreases, remaining relatively constant until an overall pressure ratio of approximately 0.27-0.30 is achieved where